Effect of Spheroidization and Inoculation on the Early Solidification Steps of Hypereutectic Cast Irons

Patrik Popelar, Jacques Lacaze

EFFECT OF SPHEROIDIZATION AND INOCULATION ON THE EARLY SOLIDIFICATION STEPS OF HYPEREUTECTIC CAST IRONS

Patrik Popelar
Technical Centre, SinterCast AB, Kungsgatan 2, 641 30 Katrineholm, Sweden

Jacques Lacaze
CIRIMAT, Université de Toulouse, Toulouse, France

https://doi.org/10.1007/s40962-024-01434-1

Abstract

Compacted and spheroidal graphite silicon cast irons generally have slightly hypereutectic compositions when referred to the equilibrium phase diagram. Previous studies have shown that the thermal analysis of these melts often exhibits misleading characteristics that could prevent proper process control. It was the aim of the present work to provide new results, taking into account the carbon equivalent as well as spheroidization and inoculation levels. Overall, the features of slightly and highly hypereutectic melts deduced from previous studies were confirmed, while additional information was obtained concerning the effect of spheroidization and inoculation levels.

Keywords: *thermal analysis, compacted graphite iron, inoculation, spheroidizing treatment*

Introduction

Industrial compacted graphite (CGI) and spheroidal graphite (SGI) silicon cast irons have slightly hypereutectic compositions—when referring to the equilibrium phase diagram—for this allows achieving a fully eutectic microstructure that minimizes the risk of porosity formation. This composition shift accounts for the fact that the coupled zone of the austenite-graphite eutectic is skewed towards the graphite side, implying that the optimal composition depends on the solidification undercooling and thus on the casting conditions.

Thermal analysis (TA) is routinely used to assess melt composition based on the rule of thumb that a thermal record showing one single eutectic plateau is indicative of a fully eutectic microstructure, i.e., of a eutectic-like solidification mode. It is, however, well understood that this conclusion is valid for the solidification conditions achieved in the thermal analysis cup and the extension to complex casting shape relies on the experience of the metalcaster who needs to establish a correlation between the thermal analysis result and the (each) casting due to the different solidification conditions (e.g., cooling rate, melt oxidation, mixing patterns). The other consideration is that the iron changes between the time of the thermal analysis sample and the pouring of the casting. This includes time, temperature and fading but the biggest change is the use of in-stream inoculation. In the case of CGI with high enough carbon equivalent (CE), this late inoculation affects the undercooling and easily has the ability to change the solidification from hypoeutectic to hypereutectic mode, while often resulting in an increase in nodularity.

As a matter of fact, analysis of literature data has demonstrated that thermal analysis of hypereutectic silicon cast irons with respect to the phase diagram often shows features impeding useful conclusions to be drawn.[1] Standard thermal analysis records from single-thermocouple cups indicate that mildly hypereutectic alloys start solidifying in a narrow range of temperature. This is illustrated with the shaded rectangle in the isopleth Fe-CE section of Figure 1.[2] Further, it is hardly possible to discriminate between austenite precipitation and eutectic initiation as already pointed out by Loper et al.[3] In the highly hypereutectic

Received: 24 May 2024 / Accepted: 01 August 2024
Published online: 23 August 2024

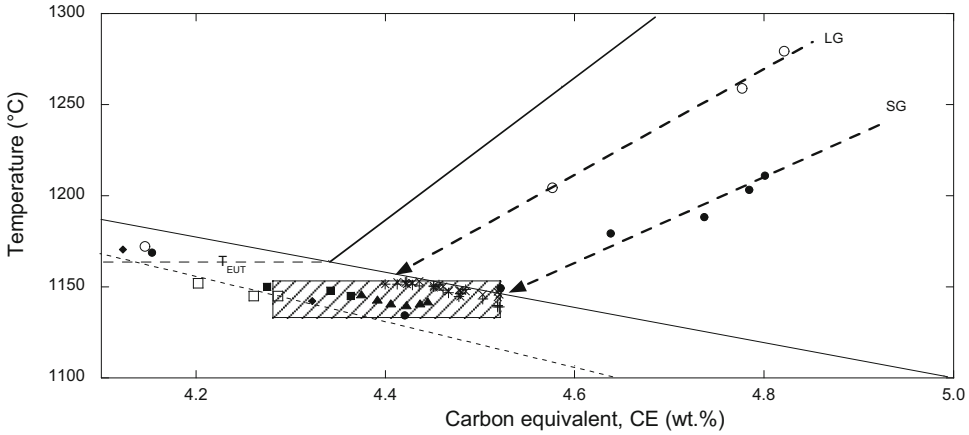

Figure 1. The Fe-CE isopleth section at 2.45 wt.% Si with symbols representing experimental temperatures for initiation of solidification from literature (see Lacaze et al.[2] for further details). The solid lines are the equilibrium liquidus for austenite and for graphite, including the metastable extrapolation of the austenite liquidus below T_{EUT}. The short-dashed line shows the best fit through Moore's data[4] for the formation of austenite. The dashed arrows labelled LG and SG go through graphite liquidus arrests from Loper et al.[3] for lamellar and spheroidal graphite precipitation, respectively. The hatched rectangle stresses the fact that slightly hypoeutectic and mildly hypereutectic alloys start solidification within a narrow range of temperature.

domain, it was noticed that the eutectic solidification starts at a temperature independent of the nominal carbon content, with the additional difficulty that primary precipitation of graphite is not always noticed. However, when this primary precipitation shows up, it does so with a high undercooling below the graphite liquidus and this difference is much larger for spheroidal graphite (SG) than for lamellar graphite (LG). This corresponds to the dashed lines with arrows for LG and SG irons in Figure 1 that also represent the related primary solidification path. The effect of the magnesium content and of inoculation was discussed based on limited information[1] and this was the objective of this project to provide new results.

Experiments were carried out using the SinterCast system that has several peculiarities: (1) the cups are made of precision formed coated steel that is immersed in the melt so as to reduce oxidation during filling; (2) the cups are equipped with two thermocouples, one at the bottom and the other at the thermal centre; (3) a coating is applied to the inner surface of the cups that consumes part of the magnesium added to the melt; (4) after the cups have been filled, the system records the temperatures of the two positions that exhibit a gradient as heat is lost from the bottom of the cup to the surroundings. This system has been devised to evaluate the modification of mildly hypereutectic alloys by means of a proprietary software that was not used in the present study. Instead, we analysed the cooling records as done in previous studies that used standard single-sensor thermal analysis cups, meaning we put emphasis on the centre records but made use of the bottom records to contrast important characteristics. Also, the aim was to investigate the early solidification steps and we will give limited information on the bulk eutectic transformation.

To achieve this investigation, five ladles with different CE contents were prepared from which castings were made at various additions of magnesium and inoculant in order to provide new information on the effect of these metallurgical parameters on the early solidification stages of mildly and strongly hypereutectic cast irons. All iron used in this study originated from the same batch of base iron where only ladle additions were used to change the chemistry. The change in CE was achieved by varying the silicon content through ladle additions of high purity silicon. Carbon content could only be adjusted in the ladle to a minor degree and thus remained relatively constant.

Experimental Details

Five ladles denoted A to E were treated to various levels of CE, Mg and inoculant addition. For this, 1000 kg of base-iron was tapped into a tundish-cover ladle, then to a pouring ladle. All iron originated from the same base iron holding furnace. Into both of these transfer processes pure silicon (Elkem Si99, 99% metallurgical grade silicon) and de-sulphurised graphite (Desulco®) were introduced before tapping. Half of each addition was added to each vessel to improve dissolution. For each ladle, four alloying steps (1–4) were performed to create four different treated iron alloys. There was no Mg addition for the first step, just carbon and silicon resulting in a grey iron microstructure. The second step was converted into CGI with the addition of cored Mg and rare-earth wire (30 g/m magnesium +

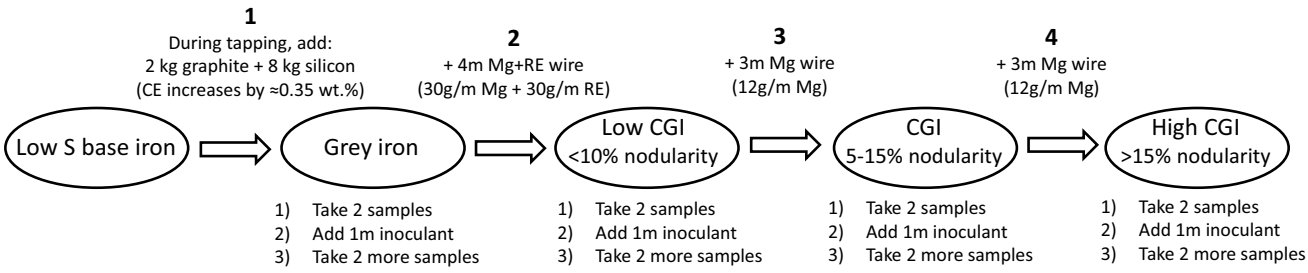

Figure 2. Example (ladle A) of the four successive alloying steps 1 to 4 with indication of the various additions. After each addition, two samples a and b were cast (e.g. A1a, A1b), an inoculant addition was made, and two more samples c and d were cast (e.g. A1c, A1d). This pattern was repeated for ladles B, C, D, and E with some occasional changes. See Table 1 for details.

30 g/m Rare Earth Mischmetal). The next two steps were adjusted by increasing the Mg content with pure Mg wire (13 g/m) and additions of inoculant (Ferroglobe ZL 80 @ 130 g/m). Just after each step, two samples, a and b, were cast, a small constant addition of inoculant was then performed and two more samples, c and d, were cast as shown in Figure 2. These small additions prevented the inoculation level from fading and also demonstrated what a small change in nucleation potential does to the resulting cooling curve. Some high additions of inoculant were also made at times to demonstrate the sole effect of inoculant on the resulting thermal curves (B3, B4, D4 and E4). Table 1 summarizes the various additions for each ladle with Mg addition indicated as "none", "low", "+", "++" or "+++". This latter very high addition of magnesium ("+++") was carried out with D4.

A chemical analysis sample was taken for each of the four different compositions of each ladle and three evaluations were made from each sample using optical emission spectroscopy (OES). The chemical results are listed in Table 1 as the average value for magnesium, carbon, and

Table 1. Ladle Identification, Intended CE and Calculated T_{EUT} and $w_{C,eut}$ Values (See Text), Treatment Step, Relative Modification Level, Inoculant Additions, Magnesium, Carbon and Silicon Contents, and Estimated CE Values

Ladle	Melt	Step	Relative modification	Inoculation	Mg	C	Si	CE
A	High CE	A1	No (grey)	0	<0.0010	3.65	3.07	4.51
	T_{EUT}=1168.8	A2	Low (CGI)	0.013%	0.0097	3.62	3.10	4.49
	$w_{C,eut}$=3.48%	A3	+	0.026%	0.0113	3.61	3.10	4.48
		A4	++	0.039%	0.0135	3.61	3.11	4.48
B	Very high CE	B1	No (grey)	0	<0.0010	3.71	3.49	4.69
	T_{EUT}=1170.0	B2	Low (CGI)	0.013%	0.0088	3.61	3.53	4.60
	$w_{C,eut}$=3.37%	B3	++	0.026%	0.0269	3.67	3.54	4.66
		B4	++	0.169%	0.0268	3.61	3.61	4.62
C	Low CE	C1	No (grey)	0	<0.0010	3.66	2.57	4.38
	T_{EUT}=1166.1	C2	Low (CGI)	0.013%	0.0092	3.72	2.42	4.40
	$w_{C,eut}$=3.65%	C3	No further Mg added	0.026%	0.0086	3.71	2.43	4.39
		C4	No further Mg added	0.039%	0.0087	3.69	2.44	4.37
D	Low CE	D1	No (grey)	0	<0.0010	3.74	2.34	4.40
	T_{EUT}=1165.7	D2	Low (CGI)	0.013%	0.0105	3.72	2.38	4.39
	$w_{C,eut}$=3.67%	D3	++	0.026%	0.0264	3.70	2.40	4.37
		D4	+++	0.169%	0.0408	3.67	2.47	4.36
E	Very high CE	E1	No (grey)	0	<0.0010	3.67	3.33	4.60
	T_{EUT}=1170.0	E2	Low (CGI)	0.013%	0.0106	3.58	3.34	4.52
	$w_{C,eut}$=3.42%	E3	++	0.026%	0.0217	3.62	3.35	4.56
		E4	++	0.169%	0.0213	3.55	3.42	4.51

Of the 4 TA samples taken, samples 'A' and 'B' were always followed by a 0.013% inoculant addition before samples 'C' and 'D' were cast.

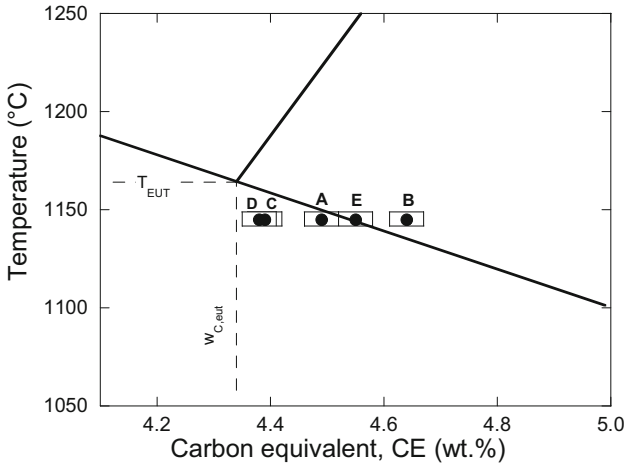

Figure 3. Positioning of the studied alloys (A to E) on a Fe-CE section as in Fig. 1. Note that the temperature scale is approximate as it depends on the silicon content of each alloy (see the various T_{EUT} temperatures in Table 1). The dots represent the average CE value for each alloy while the rectangles represent a possible error of ±0.03 wt.% corresponding to that evaluated for the average carbon content (see text).

silicon. Note that the iron alloys also contained 0.17–0.18 wt.% Mn, 0.022–0.023 wt.% P and 0.008 wt.% S, as well as very low levels of other elements. OES is not the best suited means for carbon analysis, meaning the error on individual analysis of this element could be as high as ±0.10 wt.%. Each of the values in Table 1 is the average of three measurements for which the possible error is thus ±0.07 wt.%. Similarly, if the average of the 12 analyses on each ladle is considered, the error on the carbon content will be ±0.03 wt.%, i.e., slightly better than the ±0.05 wt.% associated with a combustion analysis. Also note that all analyses were made at the same session thus ensuring relative accuracy?

In the following discussion, use will be made of isopleth Fe-C sections that were calculated with the TCFE-8 database of Thermocalc AB[5] for the indicated Si content and accounting for 0.17 wt.% Mn. The equilibrium eutectic temperature T_{EUT} and equilibrium eutectic carbon content $w_{C,eut}$ listed in Table 1 were picked up from these sections. Also, the carbon equivalent CE in Table 1 was estimated as CE = %C + 0.28 x %Si[6,7] though the use of this equation is normally restricted to silicon contents lower than 3 wt.%. This allows positioning of the alloys with respect to the equilibrium eutectic point in Figure 3 where it is seen that alloys C and D are slightly hypereutectic, alloys E and B are strongly hypereutectic, and alloy A is at the limit.

According to the labelling indicated above, each record will be denoted as Xix where X is for the ladle (A to E), i for the step (1 to 4) and x for the sample (a to d). Temperature data were recorded from the N-type SinterCast thermocouple pairs with a 16-channel low-noise analogue-to-digital converter. (Standard deviation of thermal readings at constant temperature is approximately 0.05 °C.) Each thermocouple pair is individually calibrated at an accredited testing lab to a precision of approximately 1.0 °C. A thermocouple failure prevented the recording of one sample. This along with two others that were unintentionally not filled is indicated as "Non rec." in Appendix 1.

Results

Qualitative Analysis

A primary check of all temperature records showed a high consistency of the cooling rates and solidification times with very few exceptions. Further, the small addition of inoculant between samples Xia–Xib and Xic–Xid, added to counteract accumulated fading had no significant effect on the curve shape and characteristic temperatures. Accordingly, all records Xia to Xid of any ladle X and step i could be considered as equivalent to each other.

The possibility of detecting primary graphite precipitation is expected to be easier with unmodified melts (step 1) and led to firstly compare the corresponding records of ladles A to E. This is done in Figure 4 for the first records (X1a) and it was found of interest to plot both the bottom records (Figure 4-a) and the centre records (Figure 4-b). It is clearly seen that there is a slope change during cooling before the eutectic plateau in the case of the two highly hypereutectic alloys B and E that does not occur with the mildly hypereutectic alloys C and D and should thus be related to primary graphite precipitation. This slope change occurs at slightly higher temperature in the cup centre than at its bottom. In the case of the intermediate alloy A, a slope change is identified with the centre thermocouple by drawing the time derivative of the record as shown in Figure 4-c. Compared to alloys B and E, it occurs at a lower temperature at ∼1185 °C while it is absent on the record of the bottom thermocouple.

An estimate of the amount of graphite that should precipitate at the centre position to explain the slope change for samples B1i and E1i was carried out; see Appendix 2. Considering the heat flux remains constant before and after this slope change, the change in cooling rate leads to a rate of graphite precipitation of 0.16%/s, meaning 4% (by volume) for the 25 seconds of primary precipitation in Figure 4-b. That value is quite reasonable, though being certainly an overestimate.

To study the effect of magnesium and inoculation on primary graphite precipitation, Figure 5 shows the cooling curves recorded at the centre of the four samples Bia (Figure 5-a) and Eia (Figure 5-b) where the record for C1a has also been added for reference. It is seen that with

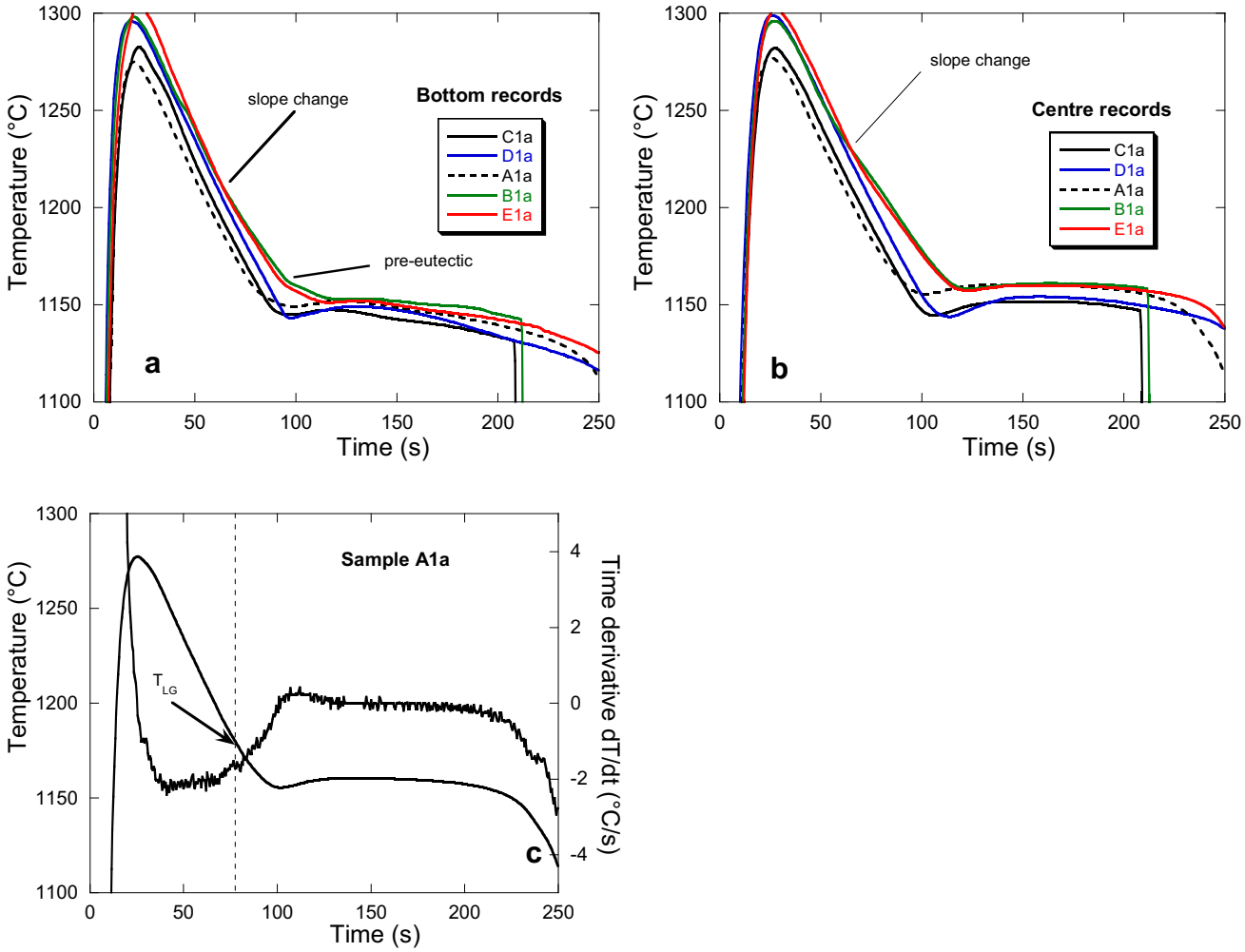

Figure 4. Records X1a for the bottom (a) and centre (b) thermocouples for all unmodified melts (ladles A to E), and cooling curve and time derivative of the centre records of A1a sample where is located the start of graphite precipitation (c).

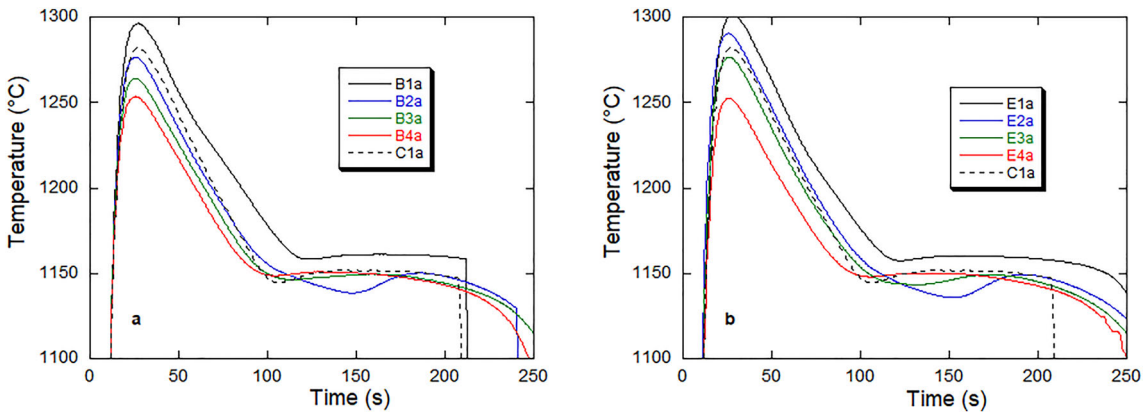

Figure 5. Effect of magnesium and inoculation on the cooling curves (centre thermocouple) of strongly hypereutectic alloys B (a) and E (b). Before Mg addition, alloys B and E demonstrate a slope change at ~1230 °C due to primary graphite formation. This distinct slope change evolves into a more gradual and subtle curvature as the graphite morphology is changed by addition of Mg. The curve for sample C1a is used as a reference when no primary graphite precipitation occurs.

adding magnesium the slope change for B2a–B4a and E2a–E4a is much less marked than in B1a and E1a and this corresponds to a slowing down of the graphite growth rate from the liquid. On the other hand, the strong inoculation in B4a and E4a may slightly affect the slope of the records during primary precipitation, but this effect is definitely minor while the effect on the eutectic transformation is important; see below.

We turn now to the next solidification step and consider first the unmodified alloys whose cooling curves are reported in Figure 4. In the cup centre, all samples showed one eutectic plateau without any marked pre-eutectic reaction other than primary precipitation of graphite for alloys A, B and E. An interesting feature is the very low recalescence of samples B and E when compared to samples C and D. (Please remember that the temperature difference between the plateaus is due to the difference in silicon content; see Table 1.) If, however, we look at the records of the bottom thermocouple (Figure 4-a), samples B and E show a pre-eutectic reaction while samples C and D still do not. Again, the intermediate sample A behaves as C and D at the bottom and B and E in the centre. Thus C and D show a eutectic mode of solidification from the bottom to the centre of the cup, while samples B and E show primary precipitation of graphite everywhere and then a pre-eutectic reaction at the bottom that disappears in the centre. Owing to the very hyper-eutectic composition of alloys B and E, this pre-eutectic reaction should relate to precipitation of both austenite and graphite but at a temperature such that the growth undercooling is not high enough for the bulk eutectic to take place.

Figure 6 shows the series of cooling records X2a for the bottom (Figure 6-a) and the centre (Figure 6-b) after the first (low) addition of magnesium that is expected to give compacted graphite in the centre of the cup. Independent of any primary precipitation, all records show that solidification proceeds in two steps, an initiation arrest followed by a eutectic plateau with significant recalescence. The main feature of the initiation arrest is that it has similar shape for all alloys, with however a sharper start for alloys C and D than for the others. The similarity of this pre-eutectic arrest supports a co-precipitation of both graphite and austenite in all samples. This co-precipitation needs, however, an increased undercooling before the bulk eutectic transformation takes place. The relative smoothness of the arrest for samples A, B and E might relate to the fact that graphite is already present in these alloys when austenite appears, while both graphite and austenite do appear together in case of alloys C and D.

Quantitative Analysis

The objective is now to characterize quantitatively the first steps of solidification of these hypereutectic alloys (referring to the equilibrium phase diagram), which means evaluating the temperature for primary graphite precipitation when it occurs (alloys A, B and E), and of eutectic or pre-eutectic reaction if any. Though focus is directed on the centre thermocouple for comparison with standard thermal analysis, limited use will also be made of the bottom thermocouple.

Starting with the low CE alloys, Figure 7-a presents the bottom and centre curves of sample C1a together with their time derivative. After the peak temperature has been reached and the associated transient finished at about 45–50 s, the curves are characterized by a slowly varying cooling rate until about 80–90 s when there is a sharp change of the dT/dt slope. This is associated with the onset of the eutectic transformation that can be characterized by the minimum temperature before recalescence, $T_{e,min}$, which corresponds to the end of the sharp slope change (see the vertical dashed lines in Figure 7-a). As pointed out above, there is no sign of any pre-eutectic precipitation and the two curves are shifted along the time axis during liquid cooling. This shift corresponds to a spatial temperature gradient that becomes more evident and marked with the

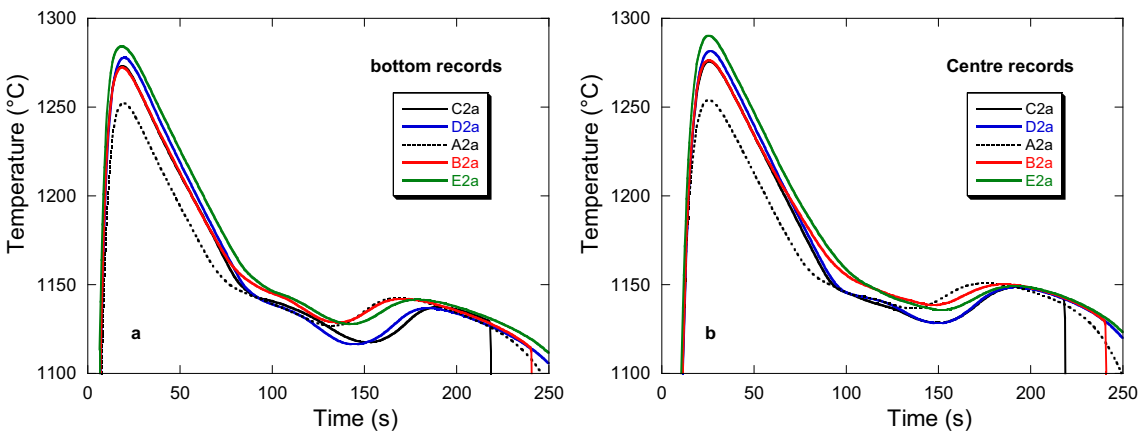

Figure 6. Records X2a for the bottom (a) and centre (b) thermocouples for low modified melts (ladles A to E).

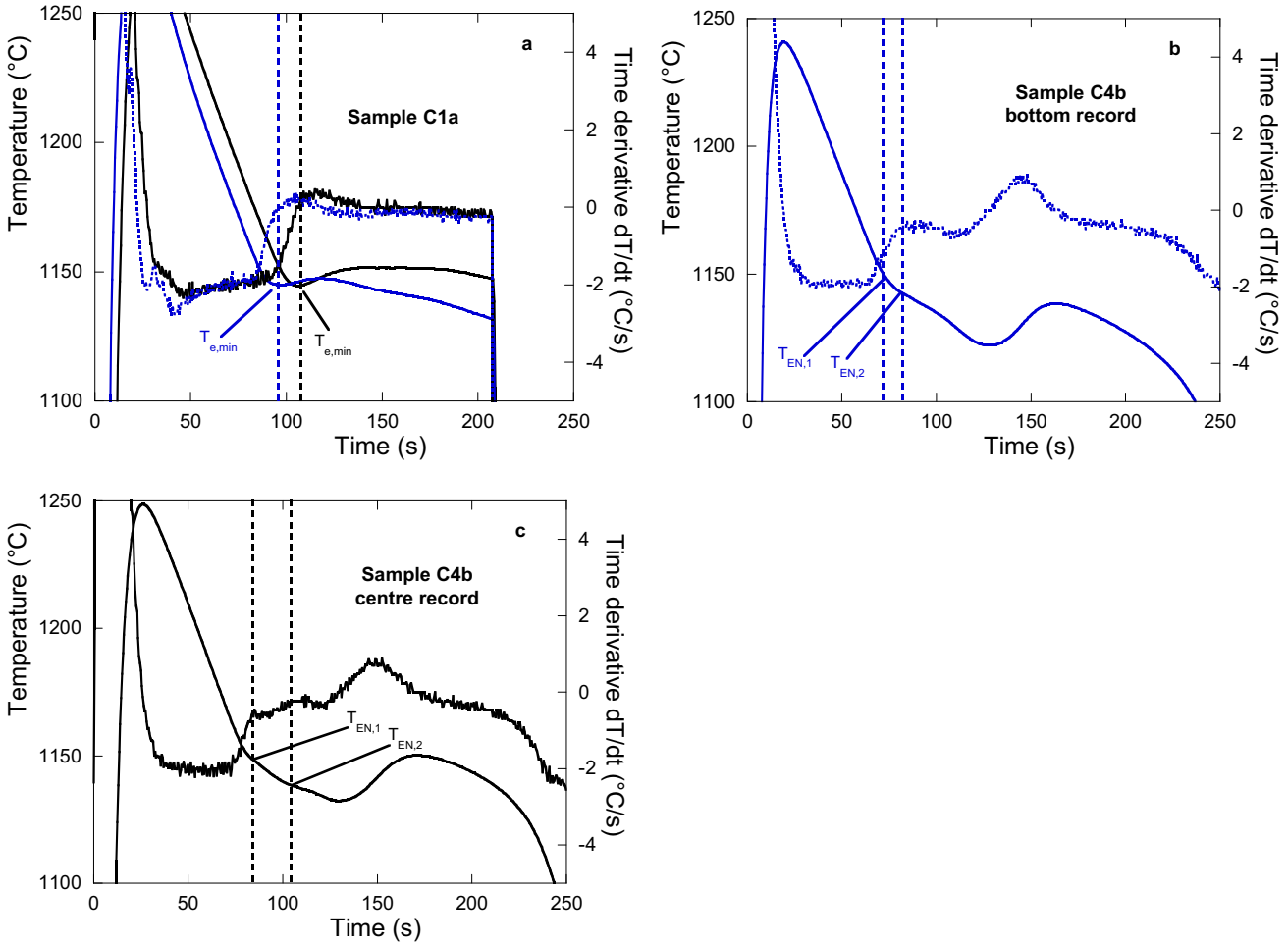

Figure 7. Cooling curves and time derivatives of bottom (blue lines) and centre (black lines) thermocouples of samples C1a (a) and C4b (b and c).

divergence of the curves during the eutectic transformation that certainly occurs when the outer surface of the cup has fully solidified. Although the cooling conditions are not exactly the same in the two locations, it is remarkable that the $T_{e,min}$ values are very similar.

Magnesium addition was made for step 2 of ladle C and no more addition was done for steps 3 and 4. As shown in Table 1, the magnesium content remained nearly constant so that all curves C2, C3 and C4 were similar and the bottom and centre curves of sample C4b are shown as example in Figure 7-b and c, respectively. As indicated above, the addition of magnesium made the solidification of this alloy to proceed in two main steps but some curves showed additional faint arrests. For the bottom thermocouple, a faint arrest could be observed during the sharp slope change and the first solidification step was thus characterized with the two temperatures $T_{EN,1}$ and $T_{EN,2}$ with this latter corresponding to the end of the slope change; see Figure 7-b. In case the first faint arrest did not show up, only the $T_{EN,2}$ temperature was reported for bottom thermocouple. All temperatures are listed in Appendix 1.

For the centre thermocouple, no faint arrest is evident during the sharp slope change on any of the records. Accordingly, the pre-eutectic arrest was characterized only with $T_{EN,1}$ that was set to the temperature corresponding to the upper end of this sharp slope change (Figure 7-c). Additional small arrests could be observed at lower temperature such as the $T_{EN,2}$ arrest in Figure 7-c but were sometimes more difficult to locate than $T_{EN,1}$. Accordingly, the pre-eutectic arrest for the central part of the cup was characterized only with $T_{EN,1}$.

The characteristic temperatures for the onset of solidification of all samples from ladle C are plotted in the Fe-C isopleth section at 2.47 wt.% Si of Figure 8. For the samples of step 1, there was no pre-eutectic arrest so $T_{e,min}$ was used. For the next steps, the reported temperatures are $T_{EN,1}$ for the centre thermocouple and both $T_{EN,1}$ and $T_{EN,2}$ for the bottom thermocouple. Focusing first on the centre data, it is seen that the $T_{EN,1}$ values of the centre thermocouple are at about the same temperature as the $T_{e,min}$ value of step 1. This is emphasized with the horizontal arrow that points to the corresponding liquid composition along the extrapolation of the austenite liquidus. It is thus

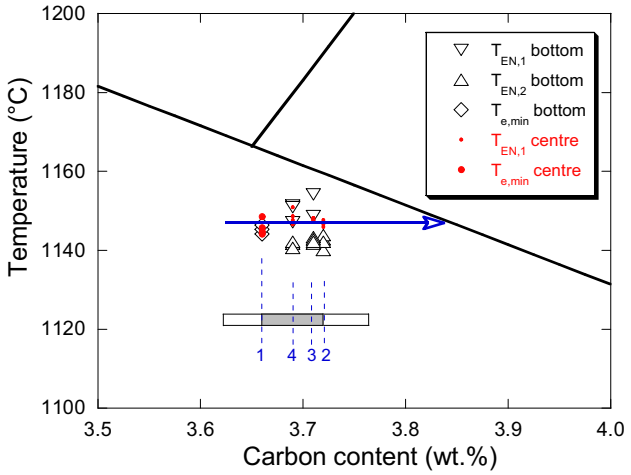

Figure 8. Characteristic temperature for the onset of solidification of samples from ladle C in the isopleth Fe-C section at 2.47 wt.% Si and 0.17 wt.% Mn. The numbers refer to the step, both bottom and centre data are shown. $T_{e,min}$ values are used when no T_{EN} arrest was present. The open rectangle has a width of ±0.07 wt.% (relates to the composition at each step) and the greyed one ±0.03 wt.% (relates to the mean composition of the ladle).

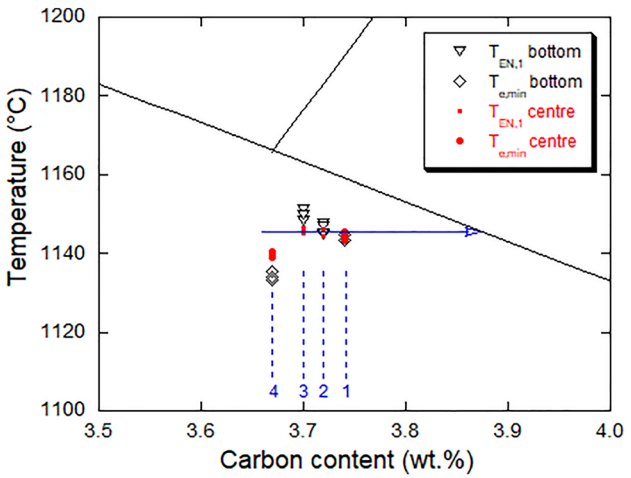

Figure 9. Characteristic temperature for the onset of solidification of samples from ladle D in the isopleth Fe-C section at 2.40 wt.% Si and 0.17 wt.% Mn. The numbers refer to the steps, both bottom and centre data are shown. $T_{e,min}$ values are used when no T_{EN} arrest was present.

straightforward to associate the $T_{EN,1}$ arrest of the centre thermocouple to the onset of the eutectic transformation, though further cooling is needed for bulk eutectic solidification after Mg addition.

Observed $T_{EN,1}$ and $T_{EN,2}$ values of the bottom thermocouple are, respectively, above and below the $T_{e,min}$ value of both centre and bottom locations of step 1. This suggests that $T_{EN,1}$ relates to austenite-precipitation and $T_{EN,2}$ to eutectic initiation. Thus, solidification is likely to proceed with an array of austenite dendrites followed by a eutectic front from the cup surface, but this evolves in one single solidification front in the central part of the cup.

Alloy D had similar CE values as alloy C, but magnesium was added at each step to reach a high value of 0.04 wt.% at step 4. At this last step a significant amount of inoculant was added along with magnesium. The records for step 1 to 3 were quite similar to those of alloy C, with only one eutectic plateau for step 1 and a two-step solidification for steps 2 and 3. The values for the solidification onset are reported in Figure 9 in the Fe-C isopleth section at 2.40 wt.% Si. As for alloy C, it is seen that the centre thermocouple gave similar values for steps 1, 2 and 3 as underlined with the horizontal solid arrow.

After significant addition of magnesium and inoculant, the samples of step D4 showed only one eutectic plateau in both locations, bottom and centre. At the level of magnesium added, it is expected that the whole of the cup solidified as SGI, and it is noteworthy that the $T_{e,min}$ temperature for these samples is significantly lower than the characteristic temperatures measured for the three first steps. Because of the strong inoculation, it is likely that the array of austenite dendrites forming at the surface of the cup became very quickly overcome by the prolific development of graphite spheroids and their austenite envelope. Accordingly, even the bottom thermocouple did not record any pre-eutectic T_{EN} arrest, and the alloy showed a eutectic-like behaviour with solidification proceeding along one single plateau.

At slightly higher CE values, samples A1a and A1b showed a faint arrest in the cup centre corresponding to primary precipitation of graphite as illustrated in Figure 4-c

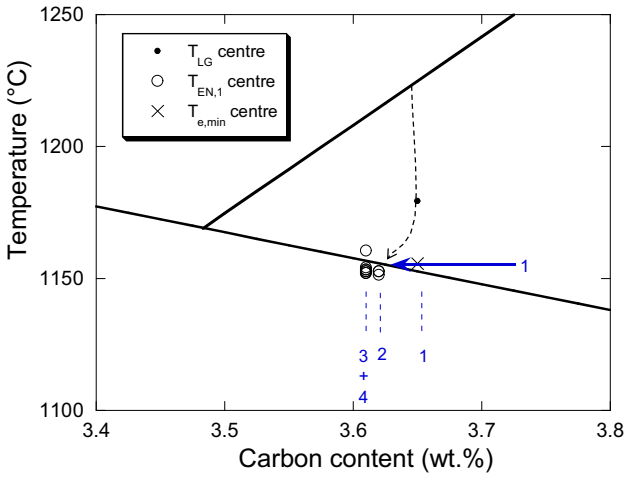

Figure 10. Characteristic temperature for the onset of solidification of samples from ladle A in the isopleth Fe-C section at 3.10 wt.% Si and 0.17 wt.% Mn. The numbers refer to the steps, only centre data are shown. $T_{e,min}$ values are used when no T_{EN} arrest was present.

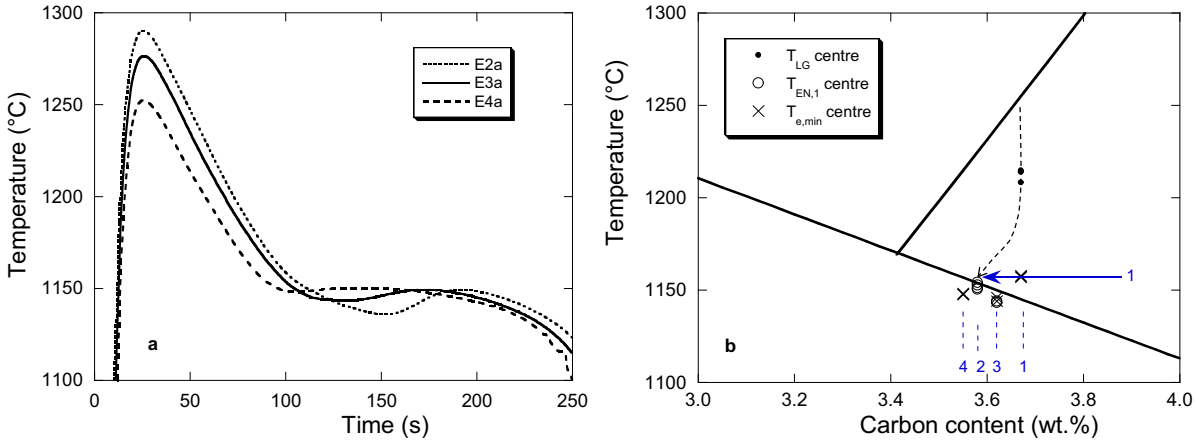

Figure 11. (a) Cooling curve of centre thermocouple of samples E2a, E3a and E4a. (b) Characteristic temperature for the onset of solidification of samples from ladle E in the isopleth Fe-C section at 3.36 wt.% Si and 0.17 wt.% Mn. The numbers refer to the steps, only centre data are shown. $T_{e,min}$ values are used when no T_{EN} arrest was present.

with sample A1a. The corresponding temperature is denoted T_{LG}. Samples A1c and A1d were not recorded but would certainly have shown the same feature. After addition of magnesium in steps 2 to 4, the records were similar to those of alloys C and D showing a two-step solidification with sometimes an additional faint arrest. The characteristic temperatures for the onset of solidification in the centre of all A samples have been plotted onto the isopleth section at 3.10 wt.% Si in Figure 10. It is seen that the $T_{e,min}$ value for samples A1 and the $T_{EN,1}$ values for samples A2 to A4 are all quite similar and closely correspond to the location along the austenite liquidus pointed with the horizontal arrow. The curve dashed line represents the possible primary solidification path of samples A1 according to which graphite precipitation leads to a decrease of the carbon content in the liquid whose composition follows a path located below the graphite liquidus. This has been previously described in detail.[1]

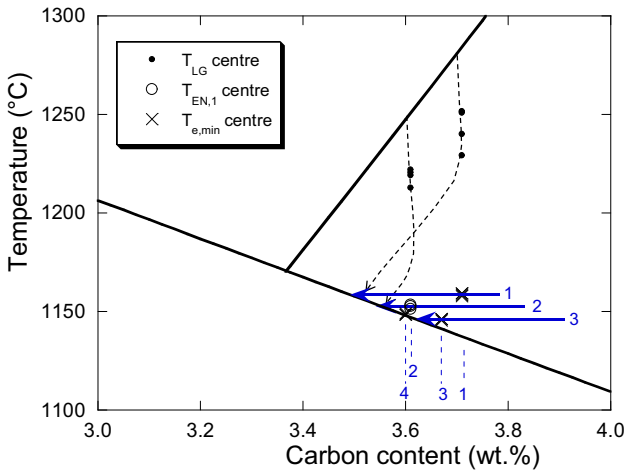

Figure 12. Characteristic temperature for the onset of solidification of samples from ladle B in the isopleth Fe-C section at 3.54 wt.% Si and 0.17 wt.% Mn. The numbers refer to the steps with data for step 4 reported at 3.60 wt.% C instead of 3.61 wt.% so as to differentiate them from step 2 values. Only centre data are shown. $T_{e,min}$ values are used when no T_{EN} arrest was present.

With further increase in CE values, the samples of alloy E appeared very much similar to those of alloy A. However, the effect of very strong inoculation in samples E4 was to suppress the pre-eutectic step as can be checked by comparing E3a and E4a centre records in Figure 11-a. When plotted in the Fe-C section at 3.36 wt.% Si of Figure 11-b, the $T_{EN,1}$ values for samples E2 and E3 are again very close to the $T_{e,min}$ values for samples E1 and E4. The dashed curve shows the suggested primary solidification path of samples E1 that ends on the austenite liquidus where points the horizontal arrow.

Finally, ladle B provided the highest CE values of the present work and the results for the onset of solidification in the centre are plotted in the Fe-C isopleth section at 3.54 wt.% Si of Figure 12. It is seen that primary precipitation of graphite could be observed also on the low modified B2 alloy (step 2) and not only on the unmodified B1 alloy (step 1). It is noteworthy that the temperature for the onset of eutectic transformation decreases with addition of Mg at constant inoculation level, steps 1, 2 and 3, in direct relation with the slowing down of graphite growth rate during primary precipitation. The strong inoculation at step 4 without additional magnesium slightly increases this onset temperature, indicative of a small effect of inoculation on primary precipitation of graphite.

Discussion

All above results for the onset of eutectic solidification in the centre of the cup, meaning either T_{EN} or $T_{e,min}$ values

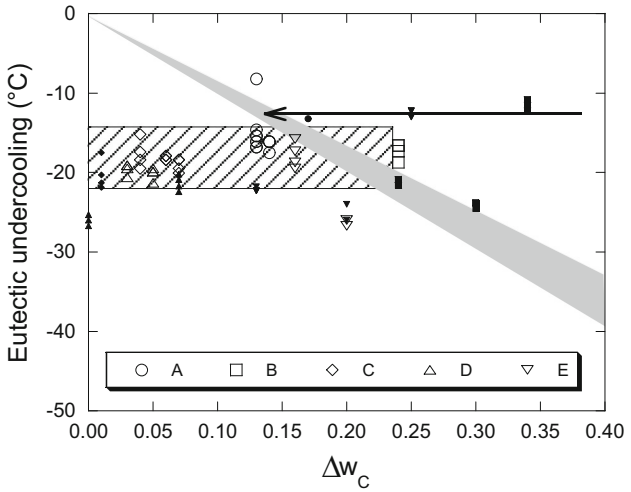

Figure 13. Eutectic undercooling data for eutectic solidification onset recorded with the centre thermocouple with various symbols for differentiating the alloys. Solid symbols are for ΔT_{EUT} calculated from $T_{e,min}$ values, open symbols for ΔT_{EUT} calculated from T_{EN} values. $T_{e,min}$ values were used when no T_{EN} arrest could be identified.

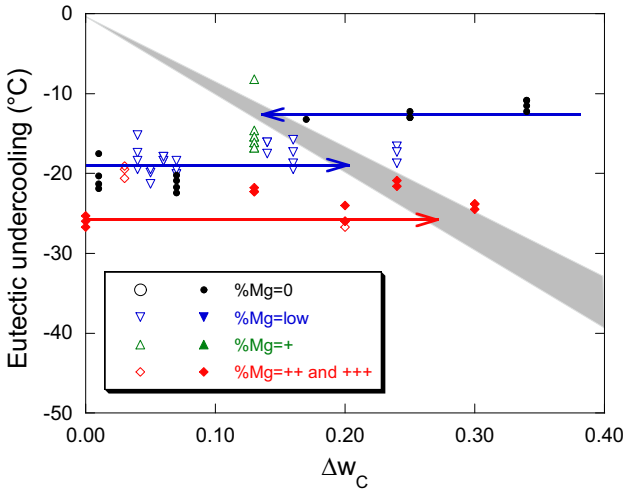

Figure 14. Eutectic undercooling data for eutectic solidification onset recorded with the centre thermocouple with various symbols for differentiating the magnesium content. Solid symbols are for ΔT_{EUT} calculated from $T_{e,min}$ values, open symbols for ΔT_{EUT} calculated from T_{EN} values. $T_{e,min}$ values were used when no T_{EN} arrest could be identified.

and excluding T_{LG} values, are reported in Figures 13 and 14 as eutectic undercooling ΔT_{EUT} versus excess carbon Δw_C with respect to the equilibrium eutectic temperature and composition. ΔT_{EUT} and Δw_C have been evaluated for each alloy using the T_{EUT} and $w_{C,eut}$ values listed in Table 1. In Figures 13 and 14, the line corresponding to the extrapolation of the austenite liquidus has been replaced with a greyed triangle to account for its slope change with silicon content. In Figure 13, the hatched rectangle emphasizes the fact that mildly hypereutectic alloys start eutectic solidification within a quite narrow range of undercooling. Loper et al.[3] described it as the austenite liquidus arrest and the eutectic start arrest merging together. There is an outlier above it from alloy A and a few results below this rectangle that will be discussed later. It is noteworthy that most of the data in this rectangle are for ΔT_{EUT} calculated from T_{EN} values, which explains why the arrest can have so often been associated with precipitation of austenite only. In the highly hypereutectic range, unmodified alloys A, B and E show nearly equal ΔT_{EUT} calculated from $T_{e,min}$ values (along the arrow pointing to the left) in relation with the expected nearly uniqueness of the solidification path during primary precipitation of graphite.[1]

The same data as in Figure 13 are plotted again in Figure 14 differentiating the samples according to the magnesium content. Most of the results enclosed in the rectangle of Figure 13 are thus associated with no, low or limited (+) magnesium content and the scatter of the data is such that no trend can be evidenced. On the contrary, magnesium contents expected to correspond to spheroidal graphite in the cup centre (++ and +++) are seen to be associated with the values located below the rectangle of Figure 13. Addition of Mg thus decreases the temperature for the onset of eutectic solidification in mildly hypereutectic alloys, while suppressing the T_{EN} arrest.

However, if the onset of the bulk eutectic transformation is considered by plotting ΔT_{EUT} calculated from $T_{e,min}$ values for all records, Figure 15 is obtained where it is clearly seen that CGI has higher undercooling than SGI. Stefanescu agreed with this result[8] but noted that Bäckerud, in an early study,[9] reported the reverse, a higher undercooling

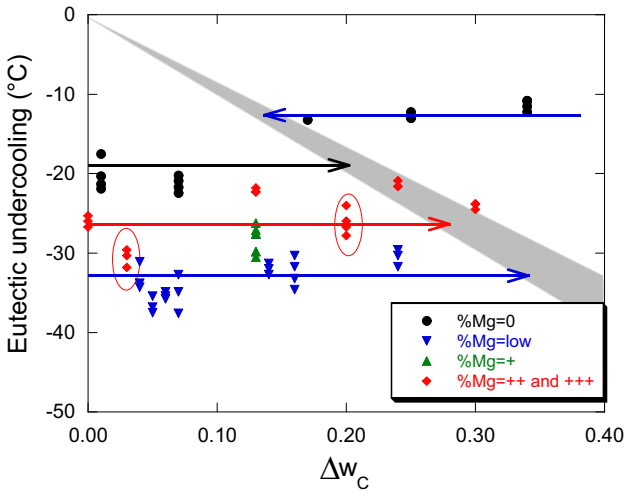

Figure 15. Maximum eutectic undercooling, $T_{e,min}$–T_{EUT}, recorded with the centre thermocouple as function of Δw_C with differentiation according to the magnesium content. The ellipses circle results for samples without extra inoculation.

for SGI than for CGI eutectic solidification. Stefanescu suggested that this inversion could be due to the use of steel cups (covered on both sides with a thin layer of alumina) by Bäckerud instead of the sand cups he used. The present work as others before[10] shows CGI has higher eutectic undercooling in metal cups, hence some other reason should be found that could be the inoculation level.

Indeed, undercooling and modification trade-off for each other and the same microstructure can be established by using a combination of high inoculant and low modification or high modification and low inoculant in the case of CGI. This counter effect can be understood in quite a simple way if one remembers that solidification of industrial CGI (with high enough CE value) starts with precipitation of graphite spheroids and makes the two following assumptions: (1) the size of the primary spheroids decreases with increase in magnesium content; (2) only precipitates that are large enough will show the protuberances needed for compacted graphite to develop. At high modification, strong inoculation will lead to numerous small spheroids when austenite appears—leading to bulk eutectic solidification similar to that of SGI—while low inoculation will give large spheroids that will easily expand with protuberances coupling with austenite. In this latter case, the few compacted graphite cells that have developed will need a high undercooling for significant growth to take place and for the strong recalescence characteristic of CGI to show up.[11] At low modification, the growth of primary spheroids will be enhanced so that protuberances may form easily and couple with austenite even in case of high inoculation. The drawback is the risk of mottling in case of insufficient inoculation.

Conclusion

A study using thermal analysis has been conducted on hypereutectic cast irons with various silicon contents, leading to an excess carbon with respect to the equilibrium eutectic in the range of 0–0.35 wt.%, i.e. from eutectic to mildly and strongly hypereutectic composition. Five alloys were prepared that were then cast after four different additions of spheroidizer and of inoculant, representative of LGI, CGI with low nodularity, CGI with high nodularity and SGI. The microstructures were not checked but guessed on the basis of SinterCast knowledge supported by the thermal records used in the present work.

Use was made of the thermal analysis cup developed by SinterCast that is equipped with two thermocouples, a so-called bottom one close to the outer surface of the cup and a centre one located in the middle of the cup. Furthermore, the inner surface of the cups is coated with a mild oxidiser that consumes part of the spheroidizer added to the melt. Together with the temperature gradient that develops during solidification, the two thermocouples give different information and emphasis was put here on the centre records focusing on the early stages of solidification. The results confirm previous investigation conducted with sand cups equipped with a single-centre thermocouple and can be summarized as follows:

- For mildly hypereutectic composition, the formation of austenite merges with the start of the eutectic reaction, and the associated eutectic undercooling is within a limited range of value, between 15 and 23 °C. Comparison with the reading from bottom thermocouple suggests that the array of austenite dendrites developing from the surface of the cup is eventually caught by the start of the eutectic reaction. In other words, dendrites and eutectic grow side by side in the central part of the cup and the thermocouple reading is in most cases unable to give any temperature difference between the two solidification fronts.
- Strongly hypereutectic alloys undergo primary precipitation of graphite that appears as a slope change on the thermal record in the case of untreated melt. On the contrary, it is not often evidenced after a spheroidizing treatment because of the associated slowing down of graphite growth rate. This primary growth of graphite is however always noticed by the fact that the temperature for the start of the eutectic reaction corresponds to a point along the extrapolation of the austenite liquidus located at a lower carbon (or CE) content than the nominal alloy composition. Addition of spheroidizer lowers the corresponding temperature (increases the undercooling) while inoculation slightly increases it.

Funding

No funding was received for conducting this study.

Appendix 1

Characteristic temperatures (°C) were measured on the bottom and centre thermocouples. The undercooling calculated with respect to the eutectic temperature T_{EUT} (see Table 1) and used in Figures 13, 14 and 15 are also listed (Tables 2, 3, 4, 5, 6). They are:

- the undercooling for the start of the eutectic reaction, $\Delta T_{EN} = T_{EUT} - T_{EN,1}$
- the maximum undercooling before the eutectic plateau, $\Delta T_{max} = T_{EUT} - T_{e,min}$.

Table 2. Ladle A

	Bottom		Centre				
	$T_{EN,2}$	$T_{e,min}$	T_{LG}	$T_{EN,1}$	ΔT_{EN}	$T_{e,min}$	ΔT_{max}
1a	1156.3	1149.1	1179.4			1155.6	13.2
1b	1166.3	1150.5	1179.4			1155.6	13.2
1c Not rec.							
1d Not rec.							
2a	1149.8	1126.7		1152.7	16.1	1136.1	32.7
2b	1152.7	1124.5		1152.7	16.1	1136.1	32.7
2c	1154.9	1128.2		1151.3	17.5	1136.8	32.0
2d	1152.7	1128.2		1152.7	16.1	1137.5	31.3
3a	1158.5	1128.9		1152.7	16.1	1139.0	29.8
3b	1154.9	1129.6		1152.0	16.8	1138.3	30.5
3c	1161.4	1129.6		1153.4	15.4	1139.0	29.8
3d	1154.2	1130.3		1154.2	14.6	1141.2	27.6
4a	1153.4	1133.0		1160.6	8.20	1141.2	27.6
4b	1152.0	1133.6		1152.7	16.1	1141.7	27.1
4c	1162.1	1132.5		1153.4	15.4	1141.2	27.6
4d	1157.0	1134.1		1152.0	16.8	1142.6	26.2

Table 3. Ladle B

	Bottom				Centre				
—	T_{LG}	$T_{EN,1}$	$T_{EN,2}$	$T_{e,min}$	T_{LG}	$T_{EN,1}$	ΔT_{EN}	$T_{e,min}$	ΔT_{max}
1a	1251.6	1159.9		1152.7	1229.2			1157.8	12.2
1b	1243.0	1160.6			1251.6			1159.2	10.8
1c	1243.7	1159.2			1240.1			1158.5	11.5
1d	1258.8	1159.9			1250.9			1159.2	10.8
2a		1154.2		1128.2	1219.1	1151.3	18.7	1138.3	31.7
2b		1159.9		1131.8	1222.0	1153.4	16.6	1139.7	30.3
2c		1155.6	1149.1	1131.0	1220.6	1153.4	16.6	1140.4	29.6
2d		1157.8	1146.9	1131.0	1212.9	1152.7	17.3	1140.4	29.6
3a				1139.7				1146.2	23.8
3b				1140.4				1146.2	23.8
3c				1139.0				1145.5	24.5
3d		1140.4		1139.0				1146.2	23.8
4a				1144.0				1148.4	21.6
4b				1145.5				1149.1	20.9
4c				1144.8				1149.1	20.9
4d				1144.0				1148.4	21.6

Table 4. Ladle C

	Bottom			Centre				
	$T_{EN,1}$	$T_{EN,2}$	$T_{e,min}$	$T_{EN,1}$	ΔT_{EN}	$T_{EN,2}$	$T_{e,min}$	ΔT_{max}
1a			1144.2				1144.2	21.9
1b			1145.3				1145.8	20.3
1c			1145.3				1144.8	21.3
1d			1146.4				1148.6	17.5
2a		1142.8	1117.1	1146.0	20.1		1128.5	37.6
2b		1143.9	1117.7	1147.7	18.4		1128.5	37.6
2c		1140.1	1123.6	1147.7	18.4		1133.4	32.7
2d		1142.2	1119.9	1146.6	19.5	1139.0	1131.2	34.9
3a		1143.3	1120.4	1147.7	18.4	1139.5	1130.3	35.8
3b	1148.7	1141.7	1119.3	1148.2	17.9	1140.1	1130.7	35.4
3c	1154.2	1142.8	1120.9	1147.7	18.4	1139.0	1131.2	34.9
3d		1142.2	1120.4	1148.2	17.9	1140.1	1131.2	34.9
4a	1151.4	1141.7	1122.0	1146.6	19.5	1137.9	1131.8	34.3
4b	1150.9	1142.2	1122.0	1148.7	17.4	1139.5	1132.3	33.8
4c	1150.9	1142.2	1124.7	1150.9	15.2	1139.0	1135.0	31.1
4d	1147.1	1140.6	1124.2	1147.7	18.4	1137.4	1135.0	31.1

Table 5. Ladle D

	Bottom		Centre			
	$T_{EN,2}$	$T_{e,min}$	$T_{EN,1}$	ΔT_{EN}	$T_{e,min}$	ΔT_{max}
1a		1143.3			1143.3	22.4
1b		1144.8			1145.5	20.2
1c		1143.3			1144.0	21.7
1d		1144.8			1144.8	20.9
2a	1147.7	1115.9	1144.4	21.3	1128.2	37.5
2b	1144.8	1118.1	1145.8	19.9	1128.9	36.8
2c	1146.9	1118.1	1145.8	19.9	1128.9	36.8
2d	1145.1	1118.8	1146.2	19.5	1130.3	35.4
3a	1149.8	1126.0	1145.1	20.6	1133.9	31.8
3b	1148.4	1126.7	1146.2	19.5	1135.4	30.3
3c	1151.3	1126.7	1146.6	19.1	1135.4	30.3
3d	1149.8	1126.7	1146.6	19.1	1136.1	29.6
4a		1133.9			1139.0	26.7
4b		1135.4			1140.4	25.3
4c Not rec.						
4d		1133.2			1139.7	26.0

Table 6. Ladle E

	Bottom			Centre				
	T_{LG}	$T_{EN,2}$	$T_{e,min}$	T_{LG}	$T_{EN,1}$	ΔT_{EN}	$T_{e,min}$	ΔT_{max}
1a	1196.8	1160.6	1151.3	1214.8			1157.0	13.0
1b	1210.5	1160.6	1152.7	1214.1			1157.8	12.2
1c	1202.5	1161.4	1154.2	1208.3			1157.8	12.2
1d	1200.4	1158.5		1214.1			1157.0	13.0
2a	1185.2	1155.6	1127.4		1151.3	18.7	1135.4	34.6
2b	1250.2	1157.8	1127.4		1154.2	15.8	1136.8	33.2
2c		1154.2	1131.0		1152.7	17.3	1139.7	30.3
2d		1154.2	1128.2		1150.5	19.5	1138.3	31.7
3a		1155.6	1133.2		1144.0	26.0	1143.3	26.7
3b		1145.5	1136.1				1144.0	26.0
3c		1157.9	1133.0		1143.3	26.7	1142.2	27.8
3d		1156.9	1137.4				1146.0	24.0
4a		1154.2	1142.2				1147.7	22.3
4b		1155.2	1141.7				1148.2	21.8
4c		1156.9	1141.2				1147.7	22.3
4d		1157.4	1139.0				1147.7	22.3

Appendix 2

Rate of primary graphite deposition

Figure 16 shows the cooling curve of sample E1a and its time-derivative. Once heat transfer during liquid cooling has become steady, the cooling rate stabilizes at about $dT_{liquid}/dt = -2.3$ °C/s, while during precipitation of graphite after the slope change it assumes a value of about $dT_{precipitation}/dt = -1.4$ °C/s. Let us consider a volume V of a few cubic millimetres around the centre thermocouple that is assumed to be homogeneous in temperature and subject to a heat extraction rate that is nearly constant. The left- and right-hand sides of the following equation express, respectively, the heat flux before and after graphite precipitation started:

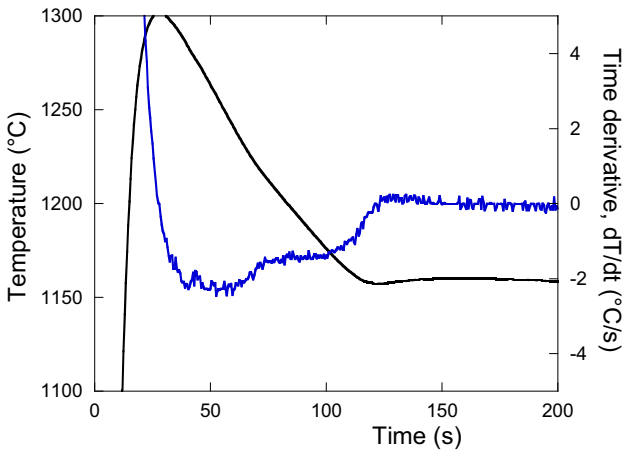

Figure 16. Plot of the temperature record and time derivative of sample E1a.

$$\rho^{\text{liquid}} \cdot V \cdot C_p \cdot \frac{dT_{\text{liquid}}}{dt} = \rho^{\text{liquid}} \cdot V \cdot C_p \cdot \frac{dT_{\text{precipitation}}}{dt} - \Delta H \cdot \rho^{\text{graphite}} \cdot V \cdot \frac{dg^{\text{graphite}}}{dt}$$

where ρ^{φ} is the density of phase φ (liquid or graphite), C_p is the specific heat of liquid cast iron (assumed unchanged by small graphite precipitation), ΔH is the heat released by graphite precipitation and g^{graphite} is the volume fraction of graphite. This equation can be rearranged to give:

$$\frac{dg^{\text{graphite}}}{dt} = \frac{\rho^{\text{liquid}} \cdot C_p}{\Delta H \cdot \rho^{\text{graphite}}} \cdot \left(\frac{dT_{\text{precipitation}}}{dt} - \frac{dT_{\text{liquid}}}{dt} \right)$$

With the density at 6800 kg/m^3 and 2200 kg/m^3 for liquid cast iron and graphite, respectively, C_p at 920 J/kg/K and ΔH at 1.62 10^6 J/kg, one gets $dg^{\text{graphite}}/dt = 1.6 \cdot 10^{-3}$ s^{-1}.

REFERENCES

1. M.J. Castro-Román, J. Lacaze, A. Regordosa, J. Sertucha, R. del Campo-Castro, Revisiting thermal analysis of hypereutectic spheroidal graphite cast irons. Metall. Mater. Trans. **51A**, 6373 (2020). https://doi.org/10.1007/s11661-020-06005-7

2. J. Lacaze, Kinetic effects on the austenite carbon equivalent and eutectic carbon equivalent of silicon cast irons. Int. J. Metalcasting **17**, 2062 (2023). https://doi.org/10.1007/s40962-022-00919-1
3. C.R. Loper, R.W. Heine, M.D. Chaudhari, Thermal analysis for structure control, in "The metallurgy of cast iron", ed. B. Lux, I. Minkoff, F. Mollard, Georgi Pub. Company, p. 639-657 (1975)
4. A. Moore, Measurement of carbon equivalent liquidus values in hyper-eutectic flake-graphite irons. Foundry Trade J. **30**, 885 (1971)
5. https://thermocalc.com/products/databases/steel-and-fe-alloys/
6. M. Castro, M. Herrera, M.M. Cisneros, G. Lesoult, J. Lacaze, Simulation of thermal analysis applied to the description of the solidification of hypereutectic SG cast irons. Int. J. Cast Metals Res. **11**, 369 (1999)
7. A. Regordosa, U. de la Torre, J. Sertucha, J. Lacaze, Quantitative analysis of the effect of inoculation and magnesium content on compacted graphite irons–experimental approach. J. Mater. Process. Technol. **9**, 11332 (2020). https://doi.org/10.1016/j.jmrt.2020.08.008
8. D.M. Stefanescu, Analysis of the rationale and accuracy of the use of carbon equivalent and thermal analysis in the quality control of cast iron. IJMC **16**, 1057 (2022)
9. L. Bäckerud, K. Nilsson, H. Steen, Study of nucleation and growth of graphite in magnesium-treated cast iron by means of thermal analysis, in "The Metallurgy of Cast Iron", ed. B. Lux, I. Minkoff, F. Mollard, Georgi Pub. Company, 1975, p. 625-637
10. S. Dawson, P. Popelar, Thermal analysis and process control for compacted graphite iron and ductile iron, Proceedings of the 2013 Keith Millis Symposium on Ductile Iron
11. J. Lacaze, A. Regordosa, J. Sertucha, U. de la Torre, Quantitative analysis of solidification of compacted graphite irons–a modelling approach. ISIJ Int. **61**, 1539 (2021). https://doi.org/10.2355/isijinternational.ISIJINT-2020-476